Journal of Sound and Vibration 401 (2017) 152–168

Contents lists available at ScienceDirect

Journal of Sound and Vibration

journal homepage: www.elsevier.com/locate/jsvi

Performance analysis of microphone array methods

Gert Herold *, Ennes Sarradj

Institute of Fluid Mechanics and Engineering Acoustics, Technische Universität Berlin, Einsteinufer 25, D-10587 Berlin, Germany

ARTICLE INFO

Article history:
Received 15 September 2016
Received in revised form
22 March 2017
Accepted 23 April 2017
Handling Editor: Prof Z Su
Available online 2 May 2017

Keywords:
Microphone array
Beamforming
Reliability

ABSTRACT

Microphone array methods aim at the characterization of multiple simultaneously operating sound sources. However, existing data processing algorithms have been shown to yield different results when applied to the same input data. The present paper introduces a method for estimating the reliability of such algorithms. Using Monte Carlo simulations, data sets with random variation of selected parameters are generated. Four different microphone array methods are applied to analyze the simulated data sets. The calculated results are compared with the expected outcome, and the dependency of the reliability on several parameters is quantified. It is shown not only that the performance of a method depends on the given source distribution, but also that the methods differ in terms of their sensitivity to imperfect input data.

1. Introduction

Microphone array methods are not merely a way to visualize acoustic sources, but an effective tool for quantitative measuring [1]. The catalog of methods for calculating source level distributions from synchronously recorded sound pressures comprises several different approaches. These include enhancements of classic beamforming techniques [2], deconvolution methods based on the beamforming result [3–5], and beamforming-independent inverse methods [6,7].

Microphone array methods map the spatial distribution of acoustic sources in terms of sound pressure level radiated towards a reference position. A desirable property of any array method is the ability to reconstruct sources with high spatial resolution, minimum artifacts and a high dynamic range. However, existing methods have been shown to perform differently depending on the given task. A previous evaluation of measurement data by Herold and Sarradj [8] revealed that different methods may yield different results even when applied to the same input from a basic experimental setup.

In the literature, many specific and exemplary comparisons of array methods can be found. Examples for experimental studies are the works conducted by Yardibi et al. [9] and by Chu and Yang [10]. While experiments are apt for yielding realistic results for the performance of the examined methods, in general, their focus is on a specific setup, whose parameters can only be varied to a very limited degree. Furthermore, with experiments, it is often not possible to define a reference with which the results obtained through a microphone array method are to be compared, which makes evaluating their performance difficult.

Using simulated data as input for the array methods has the advantage that the expected output is known and can be used as reference. Studies based on simulated input data have been done, amongst others, by Leclere et al. [11], who evaluated the qualitative differences between algorithms, and by Ehrenfried and Koop [12], who tested the algorithm

* Corresponding author.
E-mail addresses: gert.herold@tu-berlin.de (G. Herold), ennes.sarradj@tu-berlin.de (E. Sarradj).

http://dx.doi.org/10.1016/j.jsv.2017.04.030
0022-460X/

performance of methods similar to the DAMAS algorithm. However, even there, the variation of input data is generally not very extensive if existing, and the scope of possible performance evaluations therefore limited.

In addition to that, the methods compared in any evaluation, including this study, only ever represent a subset of available algorithms. This often makes a comparison with other methods difficult, in particular in the case of experimental setups.

For testing a new algorithm, it would be of advantage to be able to systematically compare its performance with other algorithms, depending on several parameters that are suspected to have an influence on the reconstruction ability. Therefore, the first objective of the present study is to provide a data generation framework that simulates typical use cases for a microphone array method but is easily extendible and adaptable. As it should allow the examination of arbitrary dependencies, a statistic approach is appropriate in order to avoid a huge number of necessary systematic parameter variations.

The second objective is to provide rating criteria to quantify the deviation of the reconstruction from the correct solution. Approaches for evaluating the calculated results differ between method-comparing studies. The most basic way consists of visually assessing the map of source levels and examine whether the represented features correspond to the expected source distribution. While this constitutes a simple way to verify whether a method works at all and to illustrate its potential differences to other methods, it depends on subjective criteria and is not suited for evaluating a high number of maps.

The spatial resolution capability of a method can be specified by evaluating the extent of the representation of a point source on a map, i.e., the sharpness of the peak, as this limits the minimum distance at which two sources appear separate. For comparing methods, a common way is to use the Rayleigh resolution limit of classic beamforming [13] as reference and calculate the minimum resolvable distance as fraction of that limit. Dougherty [14] proposed applying the Sparrow limit instead, since it is explicitly defined as the closest possible distance at which a minimum between two peaks still appears [15]. These criteria are suitable for assessing the capability of an algorithm to separate point sources of similar levels. However, they do not allow evaluating the correct reconstruction of the position and level of the sources.

As a quantitative measure of the reconstruction result, Ehrenfried and Koop [12] proposed the standard deviation of the per-grid-point difference between the reconstructed map and the correct solution. With this, both the absolute level of the sources and their positions are evaluated within a single value. However, a small error in the positioning of a source is penalized as much as a completely wrong position or even a disappearing source. Furthermore, it is not possible to separately treat the reconstruction of multiple sources in one data set.

The quantitative comparison between microphone array methods can also be done by integrating the reconstructed sound pressures over an area of interest. As the choice of the integration sectors is flexible, this approach is not limited to point sources but can be used for arbitrary source shapes [3,5,16]. The challenge here is to define integration areas in such a way that the integrated levels allow deducing meaningful information regarding the qualitative and quantitative source reconstruction ability of the methods. The approach used in this paper bears similarities with that pursued in a previous study by Herold and Sarradj [17], where the evaluation of the maps is based on integrating circular areas around point source positions.

The remainder of this paper is organized as follows. After a short summary of the microphone array methods to be compared in this study, the evaluation methodology applied here is described in detail. It consists of defining the basic setup, the rules for generating simulated data, and the approach to evaluate the maps calculated with the array methods. Subsequently, results from these evaluations are discussed, and important findings are summarized in the concluding section.

2. Microphone array methods

Microphone array methods rely on the evaluation of phase and amplitude differences of signals recorded at a number of distributed sensors. The data processing can either be done in time domain or in frequency domain [18]. The methods considered in this study work in the frequency domain and are based on the cross-spectral matrix (CSM) of the microphone signals.

The CSM is estimated using Welch's method [19]: Each time signal is divided into K blocks, onto which an FFT is applied. For each discrete frequency, the resulting complex sound pressures are stored in a vector $\mathbf{p}_k \in \mathbb{C}^M$, which has as many entries as microphone channels used. The cross-spectra between the channels are calculated and stored in matrix form for every block. Finally, the CSM is calculated by averaging all cross-spectra:

$$\mathbf{C} = \frac{1}{K} \sum_{k=1}^{K} \mathbf{p}_k \, \mathbf{p}_k^{\mathrm{H}}. \tag{1}$$

The main diagonal of the CSM contains the autospectra of the microphone channels, which hold no information about the phase differences between microphones. Since, however, its entries may contain uncorrelated self-noise of the channels from measurements, it is common to omit them in the further calculations.

The classic delay-and-sum beamformer formulation in the frequency domain is

$$b(\mathbf{x}_t) = \mathbf{h}^{\mathrm{H}}(\mathbf{x}_t) \, \mathbf{C} \, \mathbf{h}(\mathbf{x}_t), \quad t = 1 \ldots N, \tag{2}$$

where $b(\mathbf{x}_t)$ contains the squared sound pressure characterizing a source at a focus point $\mathbf{x}_t$. For acoustic source mapping, a spatial domain assumed to contain sources is discretized with a grid consisting of N focus points. The steering vector $\mathbf{h}$

contains the phase shift and the amplitude correction according to measured or modeled transfer functions from the focus points to the microphone positions. Furthermore, it fulfills the task of weighting the signals prior to the summation. Several formulations to implement this weighting exist, and the choice of $\mathbf{h}$ already constitutes a parameter that may influence the performance of a given method. Sarradj [20] showed that presently used steering vector formulations consist of a trade-off between correct reconstruction of the location and the source strength. Four different formulations were compared.

For the purpose of this study, only the third formulation was considered, which ensures a correct calculation of the sound pressure levels. Assuming a monopole sound propagation model, the entries of $\mathbf{h}$ are calculated via

$$h_m = \frac{1}{r_{t,0} r_{t,m} \sum_{l=1}^{M} r_{t,l}^{-2}} \mathbf{e}^{-\mathrm{j}k(r_{t,m}-r_{t,0})}, \quad m = 1 \ldots M, \tag{3}$$

with $r_{t,m}$ being the distance from one focus point to the m-th of M microphones and $r_{t,0}$ the distance from the focus point to an arbitrary reference position, at which the sound pressure levels are evaluated. For convenience, the reference point is set to be at the array center.

Depending on the distribution of microphones and focus points, the sound source map calculated with Eq. (2) features side lobes. These artifacts reduce the spatial resolution of the map and can be interpreted as a convolution of the correct source distribution with a point spread function intrinsic to the array geometry and the focus grid.

Several algorithms to deconvolute the map have been proposed. Here, three deconvolution methods are considered (Sections 2.1–2.3), as well as one inverse method (Section 2.4), which does not rely on beamforming techniques.

2.1. DAMAS

The algorithm proposed by Brooks and Humphreys [3] aims to reconstruct the correct source level distribution $\mathbf{b}'$ by solving the system of equations

$$\mathbf{b} = \mathbf{P}\mathbf{b}', \tag{4}$$

where $\mathbf{b}$ is a vector with N entries, containing the output of Eq. (2). The columns of the matrix $\mathbf{P}$ contain the point spread functions from each focus point to all other focus points. Eq. (4) is solved with a modified Gauss-Seidel algorithm, enforcing the non-negativity of the result.

2.2. Orthogonal beamforming

The method was introduced by Sarradj [5] and is based on the assumption that portions of the measured data that can be attributed to uncorrelated sources can be revealed by an eigendecomposition of the CSM. The beamforming is done for each component separately, i.e., the matrix $\mathbf{C}$ in Eq. (2) is replaced by $\mathbf{v}_i \lambda_i \mathbf{v}_i^{\mathrm{H}}$, with $\mathbf{v}_i$ and λ_i describing the i-th eigenvector and eigenvalue respectively. Source maps are generated for selected eigenvalues, and the maxima of the maps are compiled into a combined map to represent the source distribution. The number of sources in the final map is determined by the number of eigenvalues considered in the data processing – at the most as many as microphones used. In the evaluations performed here, the number of eigenvalues considered is set to 20, since the maximum number of sources present in any one data set is always lower (see Section 3.2.1).

2.3. CLEAN-SC

Side lobes in the classic beamforming map are coherent to the sources causing them. Sijtsma's CLEAN-SC algorithm [4] makes use of this. The idea is to search for the maximum in the convoluted map and store it in a new (clean) map. Then, the source and its coherent parts are subtracted from the original map. The process is then reiterated until no more significant sources are found or a maximum number of iterations is reached. Performance of this method is governed by a damping factor between 0 and 1 and the number of iterations. With a damping factor below 1, only a fraction of the found value and coherent portions are subtracted in each iteration step. This is needed to account for superposed sources or sources positioned in side lobes of a stronger source. However, with a lower damping factor, more iterations are needed. The choice of a damping factor of 0.6 for the calculations in this study constitutes a good compromise between the iteration number and the thoroughness of the deconvolution.

2.4. Cross-spectral matrix fitting

In contrast to the previous methods, the cross-spectral matrix fitting (CMF) is not based on beamforming, but aims to recover the source level distribution inversely from the CSM and the assumed sound propagation model. Several variants of this idea have been described in the literature [6,7,16]. Here, the source map is calculated by solving the convex optimization problem

$$\min_{\mathbf{b}'} \| \mathbf{C}_{\mathrm{vec}} - \mathbf{A}\mathbf{b}' \|_2^2 + \alpha \| \mathbf{b}' \|_1, \quad \alpha > 0. \tag{5}$$

Table 1
Microphone array method parameters.

Type of methods	CSM-based
CSM main diagonal	removed
Steering vector	Eq. (3)
DAMAS iterations	500
CLEAN-SC iterations	500
CLEAN-SC damping	0.6
OB no. of eigenvalues	20
CMF max. iterations	500
CMF regularization	BIC [22]

$\mathbf{C}_{\mathrm{vec}}$ is the vectorized lower triangular of the self-adjoint CSM with $\tilde{M} = \sum_{l=1}^{M} l$ entries, and $\mathbf{A}$ is the $\tilde{M} \times N$ transfer matrix describing the sound propagation from the focus grid positions to the microphones. The regularization parameter α is used to enforce sparsity of the solution while searching for the best possible fit for the data. The system described by Eq. (5) is solved using a Least Angle Regression Lasso algorithm [21], and α is determined applying the Bayesian information criterion [22].

All of the above microphone array methods feature one or more parameters, which have an influence on their performance. While this influence may also be studied to obtain an optimal parameter combination for the intended use case, for clarity it was chosen to set the parameters to fixed typical values. The parameter values are summarized in Table 1.

3. Evaluation methodology

The objective of this section is to provide a framework in which a given algorithm can be tested. A straight-forward way of doing this is by using data sets with known results and see whether the algorithm is capable of reconstructing the source distribution. This can be done with measured or simulated data.

With data from measurements, additional parameters and uncertainties are added to the system. These may involve, amongst others, actual source directivities not corresponding to the used models, particularities in the sound path that are not accounted for (reflections, temperature gradients, flow), or incorrect positioning of sources or receivers. Furthermore, in order to draw more general conclusions regarding the performance of an algorithm, it is necessary to test it on a sufficient variety of different data sets, which can become costly in terms of experimental efforts.

Generating simulated data sets, on the other hand, has the advantage that the input for the array methods can be forced to perfectly fit the assumptions made regarding the nature of the sources, their signals, and the sound propagation. Also, deliberate deviations from these assumptions can be introduced in a controlled manner to test the sensitivity of the algorithms to imperfect input data.

With the simulation of input data, it is possible to run a large enough number of calculations to apply a Monte Carlo method for acquiring a statistical evaluation of the performance of the algorithms. This approach was already adopted by Herold and Sarradj [17] to estimate the reliability of array methods with perfect input data. In the present study, the influence of imperfect input is evaluated additionally.

For data generation and evaluation the Acoular software package [23,24] was used, which provides tools for simulating array measurement data as well as implementations of the algorithms described in Section 2 and means for further analyzing the results. The following sections describe the details of the data generation and evaluation setup.

3.1. Environment setup

The basic setup describing the array geometry and the expected source area is kept constant for all evaluations, and only the actual data is varied (see following section).

The microphone distribution is shown in Fig. 1. The array features 64 microphones, with one microphone at the array center and the rest distributed over seven logarithmic spiral arms.

The aperture d, together with the speed of sound c, is directly coupled with the performance at chosen frequencies and the possible spatial resolution of sources. All length units in this study are normalized with the array aperture, so as to make the results applicable on a broad range of possible setups. Frequencies are described in the non-dimensional form of Helmholtz numbers

$$He = \frac{f\,d}{c}. \tag{6}$$

The focus area is chosen to be in a plane parallel to the microphone array. It is discretized by a regularly-spaced square grid with the side length equal to the array aperture, i.e., $x, y \in [-0.5\,d, 0.5\,d]$. The distance of the focus grid to the microphone array plane is set to $0.5\,d$, and the distance between the grid points is $\Delta x = \Delta y = 0.02\,d$. This results in the focus grid containing a total of $51 \times 51 = 2601$ points.

The medium is resting and homogeneous. See Table 2 for a summary of the parameters describing the environment setup.

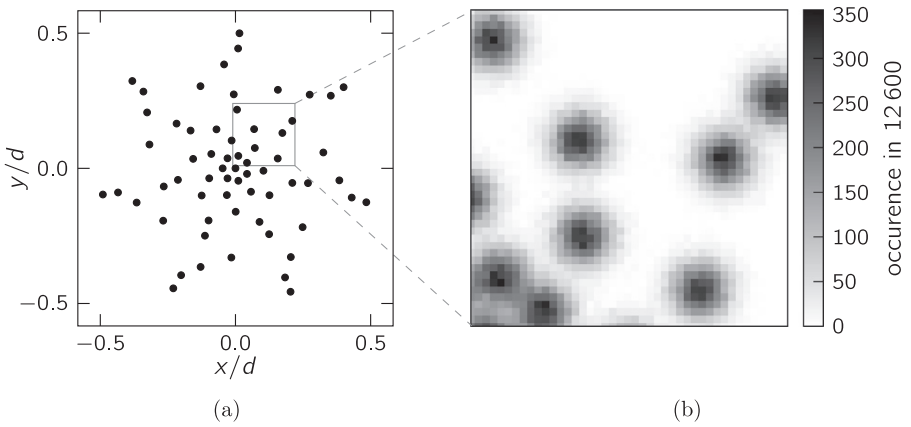

Fig. 1. Array geometry with 64 microphones in one plane, aperture *d*. Nominal positions (a) and representative section with histogram of 12,600 disturbed microphone positions (b).

Table 2
Environment parameters.

Environment	resting, homogeneous fluid
Array	7 logarithmic spirals, see Fig. 1a, 64 microphones, $z=0$
Focus grid	regularly spaced square $x, y \in [-0.5\,\mathrm{d}, 0.5\,\mathrm{d}]$, $z = 0.5\,\mathrm{d}$ $\Delta x = \Delta y = 0.02\,\mathrm{d}$

3.2. Data generation

Based on the setup described in the previous section, the methods were tested on simulated data sets. Each of the data sets models a limited number of uncorrelated monopole sources, complying with basic assumptions of the evaluation algorithms in that respect. All sources emit Gaussian white noise. In actual applications, the source characteristics may be more complex. However, it can be argued that the performance of a method applied to a well-behaved problem, in particular its failure to reconstruct the source distribution with certain parameter combinations, can be used as an indicator for the general capabilities of this method.

The use of perfect input data may hide the sensitivity of a given algorithm to small deviations from the assumed model, which could occur in measurements. However, statistically modeling possible deviations influencing the sound transfer from source to receiver is a complex task, as locally diverging fluid properties, such as density, temperature or flow, source directivity, and possible misplacement of microphones would have to be taken into account. Therefore, it was chosen to only slightly disturb the microphone positions while simulating measurement data, but to use the nominal positions in the data processing with array methods. In addition to an imperfect array geometry, this emulates in part the effect deviations in the transfer path would have.

The deviation of the simulated from the nominal microphone position $(\Delta x_m, \Delta y_m)$ is drawn from a bivariate normal distribution for each microphone and for each data set. The standard deviation of the distribution is chosen to be 1/3 of the minimum distance between two microphones. A representative histogram of microphone positions is shown in Fig. 1b.

Aside from the disturbed microphone positions, the following properties were varied for each data set:

- number of sources (positive integers)
- source positions (continuously within the focus area)
- relative source levels (continuously)

The resulting possible parameter space is quite large, especially since source positions and levels can assume an infinite amount of values. Therefore, a Monte Carlo approach is pursued here, i.e., not every possible parameter combination is evaluated, but relevant scenarios are generated by drawing the above properties from random distributions representing their expected occurrence in actual measurements. The following sections illustrate the process of generating a data set and specify the underlying distributions. A total of 12,600 data sets was generated and evaluated.

3.2.1. Number of sources

The number of sources present in a data set is drawn from a Poisson distribution. This distribution describes the probability of a given number of events (here: number of sources) occurring in a fixed interval of time or space (here: for

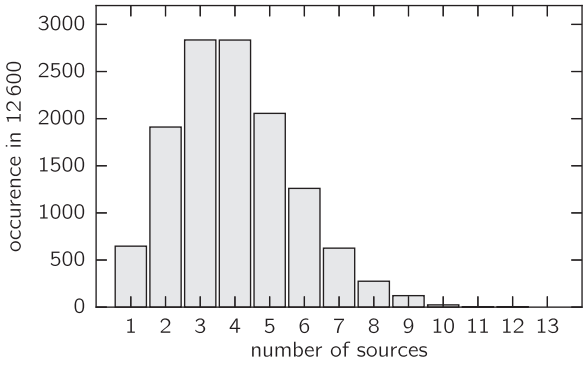

Fig. 2. Histogram for number of sources drawn from the Poisson distribution ($\lambda = 3$, 12,600 samples).

one data set and within the focus area). Possible integer values include 0, therefore a value of 1 is added to the drawn number. The rate of occurrence is set to $\lambda = 3$, so on average, four sources will be present in the data sets. Fig. 2 shows the distribution of source numbers in the simulated data sets. As can be seen, the most probable number of sources is 3 or 4. Lower or higher number are possible, but less likely. The highest number actually drawn is 12.

3.2.2. Source positions

All sources are constrained to be located in the focus plane ($z_{\text{source}} = d/2$) and within the outer borders of the focus grid ($x, y \in [-d/2, d/2]$). They do not necessarily coincide with an actual grid point. The position of each source is drawn from a bivariate normal distribution with a standard deviation of $\sigma = 0.1688$ d. With this, 2/3 of the positions lie inside the circle with a diameter of $d/2$ (see Fig. 3). If a position outside the focus area is drawn, the values are discarded and the position is redrawn.

The choice of the distribution with sources being more likely to be positioned towards the center of the focus grid appears reasonable considering actual array measurements being usually designed such that the sources of interest lie near the center of the focus area.

3.2.3. Source levels

The amplitude of a source signal can be defined by the resulting squared sound pressure p^2_{RMS} occurring at a reference distance. In the absence of spurious noise and limitations of measuring equipment, the absolute source levels are of no significance, as opposed to the relative source levels within one data set.

The sources in one data set are assumed to have different levels. While the case of the levels being in the same order of magnitude should be most probable, deviations should be allowed, however get less likely with higher magnitude. This can be achieved by drawing p^2_{RMS} of each source in one data set from a Rayleigh distribution (see Fig. 4). The scale parameter σ_{R} governs the spread of the distribution. As with relative source levels only the ratio between the Rayleigh-distributed values is of importance, the choice of σ_{R} is arbitrary.

Fig. 5 shows histograms of the minimum and maximum relative source level differences between any two sources in data sets with four sources. The minimum level difference is less than 1 dB in more than 75% of the cases, while the maximum differences are most likely to be within 2 to 8 dB.

These characteristics of the chosen random distribution are desirable, assuming that in a typical measurement case there are several sources with comparable levels, and sources with levels of 15 dB or more below any other source are of minor interest.

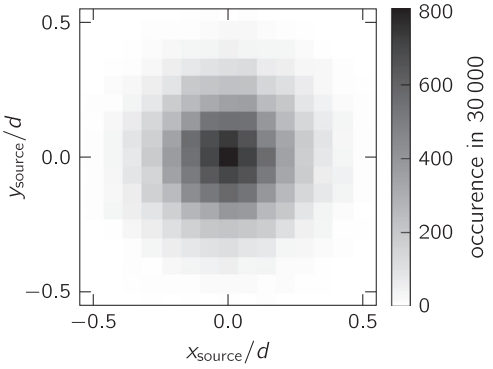

Fig. 3. 2D-histogram for 30,000 source positions drawn from the bivariate normal distribution ($\sigma = 0.1688$, values constrained to $x, y \in [-0.5\,d, 0.5\,d]$).

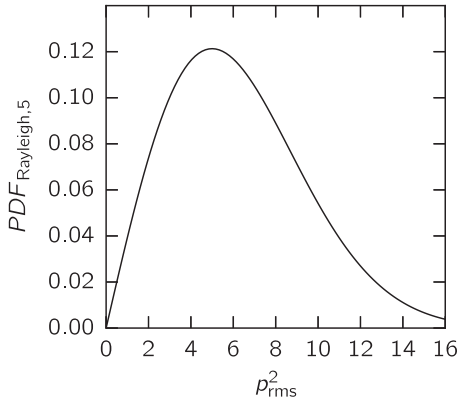

Fig. 4. Probability density function for the Rayleigh distribution (mode $\sigma_R = 5$).

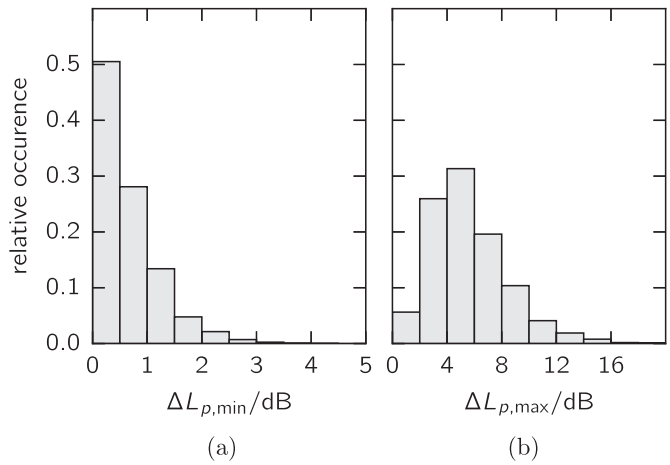

Fig. 5. Scaled histogram of the minimum (a) and the maximum (b) level differences occurring between 4 source levels randomly drawn from the Rayleigh distribution.

The simulated measurement signals at the microphone positions are sampled at a frequency corresponding to $He = 40$. For the CSM estimation as described in Section 2, each signal is divided into blocks of 1024 samples which overlap by 50%. With the time signal consisting of 512,000 samples, this results in 1000 blocks. Prior to the FFT, von-Hann windowing is applied to the blocks to diminish spectral leakage caused by the transformation. The sampling rate and block size are chosen such that the third-octave band around the lowest considered Helmholtz number $He = 1$ still contains six discrete values. The frequency resolution with this data processing is $\Delta He = 0.039$.

Important data generation parameters used in this study are listed in Table 3.

3.3. Error evaluation

One of the major objectives of this paper is to provide a simple measure for the quality of the reconstructed sound source map. The nature of the possible misrepresentation of the actual source distribution can be diverse. Not only may the calculated source levels differ from the true value. Also, the position and the extent of the sources may deviate from the truth.

With only point sources in the simulated data sets, the description of the theoretic solution is well-defined. All evaluations are based on sound source maps calculated with the microphone array methods applied onto the simulated data sets. The resulting narrow-banded maps are summarized to one-third octave bands around Helmholtz numbers between 1 and 16. For quantifying the error made by a chosen algorithm, the difference between the reconstructed and the expected sound pressure level is evaluated:

$$\Delta L_{p,\text{e}} = L_{p,\text{reconstructed}} - L_{p,\text{theoretic}}. \tag{7}$$

This will yield a single value, indicating whether the algorithm has over- or underestimated the source levels. The choice of sound pressure levels instead of pure sound pressures is motivated by their easier intuitive interpretation. Furthermore, the level difference corresponds to a ratio of the squared sound pressures, which allows comparing numerous calculations independent of the underlying absolute source levels.

Table 3
Data generation parameters.

Source type	monopole
Signals	uncorrelated white noise
Sensor positions	distorted (see Fig. 1)
No. of sources	**varied** (see Fig. 2)
Source positions	$z = d/2$; x, y **varied** (Fig. 3)
Source levels	**varied** (see Figs. 4 and 5)
Sampling rate	$He_{\text{sample}} = 40$
No. of samples	512,000
Block size	1024 samples
Block overlap	50%
Windowing	von Hann

Depending on the focus points used for the evaluation in Eq. (7), different performance measures can be deduced. In the following, three sub-sets of focus points are evaluated to calculate a characteristic level error.

3.3.1. *Overall level error* $\Delta L_{p,\mathrm{e,o}}$

Since only data sets with all sources positioned within the focus area were generated, the sum of all calculated squared sound pressures at the grid points should theoretically be equal to the sum of the squared sound pressures caused by all sources in the data set at the reference position (array center).

Only one value per map $\Delta L_{p,\mathrm{e,o}}$ is calculated, indicating the capability of an algorithm to quantify the sources. It should be kept in mind that this level error does not penalize wrong localization and only serves as a general indicator.

3.3.2. *Specific level error* $\Delta L_{p,\mathrm{e,s}}$

In contrast to the overall level error, this indicator calculates the deviation of the level for each source in a map separately. As the true source positions do not necessarily coincide with focus grid points, the squared sound pressures at grid points lying within a circle around the nominal source positions are summed. The diameter of that circle can be chosen arbitrarily and is set to 0.1 d for this study. This corresponds to the delay-and-sum beamwidth w of a central point source at the one-third octave band around $He = 8$, i.e., the distance between the opposite positions where the sound pressure level drops to 3 dB below the maximum value (see Fig. 6).

The specific level error will be non-zero if either the source level or the source position are not recovered correctly. A distinction which of the two is the case can not be made directly.

3.3.3. *Inverse level error* $\Delta L_{p,\mathrm{e,i}}$

For the previous error indicators, either the sound pressures within circles around the source positions or within the whole focus area are integrated. This allows evaluating whether an algorithm is over- or underestimating the source levels, but gives no direct information about a misrepresentation of the location of the sources. The nature of the latter can manifest in several ways, including

- scattering of single sources over a larger area
- “melding” of neighboring sources
- false detection of spurious sources by the algorithm
- any combination of these effects.

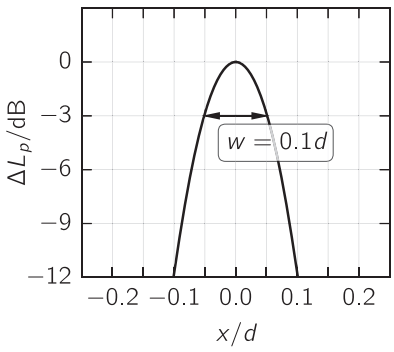

Fig. 6. Main lobe and beamwidth for the 1/3 octave band around $He = 8$.

Table 4
Evaluation parameters.

Evaluation basis	sound maps for 1/3 octave bands
Frequencies	$He_{\min} = 1$, $He_{\max} = 16$
Evaluation type	integration of map subdomains and comparison with expected results, Eq. (7)
Integration sectors	whole map, circles with diameter of 0.1 d

All these phenomena will result in the mapping of sources – partially or fully – outside the integration circles around the nominal source positions.

For a qualitatively good reconstruction, however, the premise is that all sources are contained within the source circles, i.e., the overall sound pressure level should be equal to the integrated sound pressure level of all source circles. Therefore, a location error measure can be defined based on Eq. (7) by subtracting the former from the latter:

$$\Delta L_{p,\mathrm{e,i}} = L_{p,\text{source circles}} - L_{p,\text{overall}}. \tag{8}$$

As the source circles are contained in the overall focus area, the error can only assume values equal to or below 0 dB. Any of the above-mentioned phenomena will show up in the inverse level error, with a result below zero indicating that sound pressure levels are calculated at positions where no sources are expected.

A short summary of the basic evaluation scheme is shown in Table 4.

Fig. 7 shows an example of a map calculated with the CLEAN-SC method, including the level errors introduced above. The underlying data set was generated randomly with the procedure described in Section 3.2.

With the overall level error $\Delta L_{p,\mathrm{e,o}} = 0$, the total reconstructed sound pressure levels equals the expected value. However, the negative specific level errors for all sources except source no. 3 show that the levels at those positions are underestimated. The inverse level error ($\Delta L_{p,\mathrm{e,i}} = -5$ dB) is also negative, i.e., source levels are being found outside the integration circles. Therefore, the indicators quantify the erroneous localization of the sources, which is visible in the map.

For the prediction of the general performance of an algorithm under different circumstances, the level errors are evaluated statistically in the following section.

4. Results

4.1. Computational cost

Calculations were performed on a computer cluster with 104 2.2 GHz CPUs. The overall computation time spent on the evaluations (excluding the generation of the data sets) was 61,100 CPU hours. The relative computation times are listed in Table 5.

DAMAS in its classic form is by far the most time-consuming algorithm. Exchanging the original Gauss-Seidel algorithm for solving Eq. (4) with a more efficient method would considerably speed up the calculation. However, these methods also show a different performance from the original solver in terms of source reconstruction [12,10], and therefore merit a separate examination.

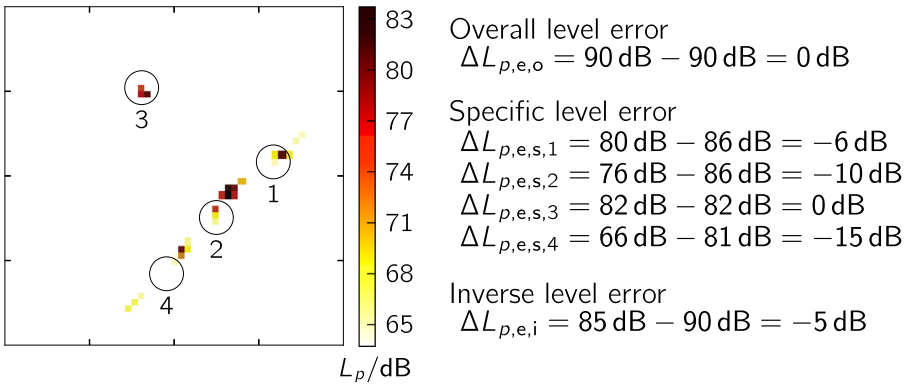

Fig. 7. Example of a CLEAN-SC map for $He = 2$, 1/3 octave. Circles indicate integration areas around the correct source positions. Also shown are the level errors calculated according to Eq. (7).

Table 5
Relative calculation time of the evaluated algorithms.

DAMAS	69.6%
OB	0.5%
CLEAN-SC	1.2%
CMF	28.7%

Furthermore, the calculation of the point spread function **P** can take an amount of time widely exceeding the time needed for calculating the actual deconvolution. In this case, the PSF calculation took about 30 times as long as the average DAMAS calculation. Since the general setup and its boundary conditions stay constant for all calculations, it had to be calculated only once for all cases and is omitted in the time evaluation. For an application in a real scenario, however, the PSF might have to be calculated more often and the time necessary for doing that can not be neglected.

The CMF algorithm is considerably faster in this case. While the DAMAS performance mostly depends on the focus grid dimensions, for CMF both the focus grid and the number of microphones are important (see Eq. (5)). On the hardware used for the calculations, an average CMF calculation took about 1.4 hours.

The calculation times of the CLEAN-SC and OB algorithms are negligible in comparison to CMF or DAMAS.

4.2. Level error evaluation

The performance of a method can be assessed by evaluating the statistical spread of the level errors. Fig. 8 shows histograms of the specific level error of the strongest source in each data set, evaluated at the 1/3 octave band around $He = 2$ and for the four microphone array methods. The bins comprise level errors within a 1 dB interval each. If the integration of the circular sector around the known source position reveals no sound pressure, the level error tends to negative infinity.

The optimal level error is zero, and for a good performance of a method it is desirable that the spread around zero is as small as possible. For all methods except Orthogonal Beamforming, the most occurring interval is represented by the bin at zero level error. The DAMAS and CMF histograms are comparatively narrow, with the vast majority of the level errors lying within an 5 dB interval around zero.

The spread of the level error distribution in the CLEAN-SC histogram is visibly higher, with a significant number of cases where no sources have been reconstructed at the nominal source position.

In case of the Orthogonal Beamforming, most of the evaluated data sets reveal no source level and an infinite level error at this Helmholtz number.

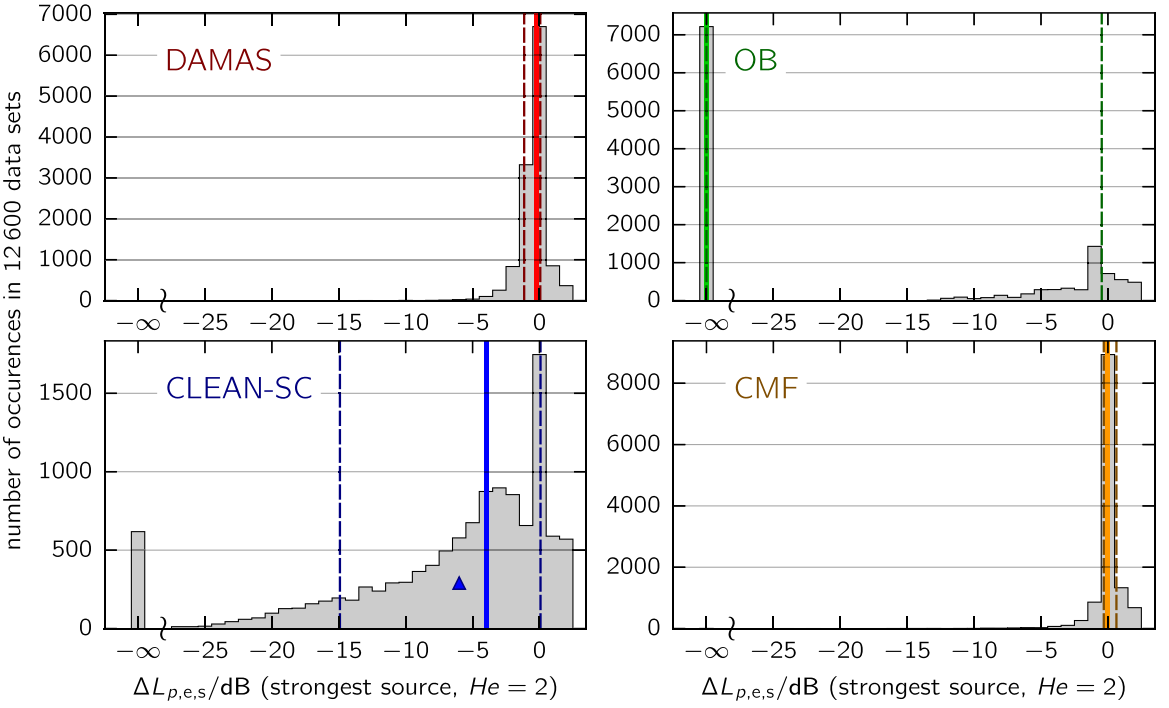

Fig. 8. Histogram of the specific level errors $\Delta L_{p,\mathrm{e,s}}$ for the strongest source in each data set at the 1/3 octave band around $He = 2$. The perpendicular lines depict the median (solid line) and the 16th and 84th percentiles (dashed lines) of the level errors. The triangle in the CLEAN-SC plot marks the bin containing $\Delta L_{p,\mathrm{e,s},1}$ from the case in Fig. 7.

The figures also show the median and the 16th and 84th percentiles of the specific level errors. In case of a normal distribution, the median would be identical to the mean of all values, and the percentiles would correspond to one standard deviation to each side of the mean.

As the interval between the percentiles contains 68% of the level errors, and the position of the median reveals possible asymmetry of the histogram, a simplified representation of the underlying error distribution and its weighting can be given by these three indicators.

In the case at hand, these show that the DAMAS and CMF algorithms perform best, with the median almost at zero and the percentiles close-by. The DAMAS error distribution is slightly broader and asymmetric towards negative values, i.e., DAMAS tends to either underestimate the source levels or slightly misrepresent the source location. In contrast, the CMF method tends to overestimate the source level in some cases. Similar to the DAMAS result, the percentiles show that in more than two thirds of all cases, the level error stays within an interval of 1 dB.

The upper and lower percentiles in the CLEAN-SC histogram reveal the spread to be 20 dB in 68% of all cases, with half of all specific level errors being below -4 dB.

With most of the level errors approaching negative infinity with the OB algorithm, the median does so as well. The 84th percentile is at approximately -0.5 dB, so in at least 16% of all cases, the algorithm is still able to reconstruct a source within the designated integration area at $He = 2$.

4.2.1. Influence of Helmholtz number

For a better understanding of the performance of the algorithms at other frequencies, the median and percentiles of the specific level errors calculated with the different methods are plotted over the Helmholtz number in Fig. 9. Here, $\Delta L_{p,e,s}$ is being evaluated for the strongest, the second-strongest, and the weakest sources in each data set. The zero-axis is shifted by 6 dB between the different methods to achieve a better visibility of the curves.

For all methods, the error drops below zero at the lowest Helmholtz number. This is not surprising, bearing in mind that all methods rely on the evaluation of phase differences between the recorded signals, and that these diminish with lower He.

However, the extent of the deviation from the correct source levels differs depending on the method and the relative strength of the source. Most prominently, the error median assumes high negative values at low Helmholtz numbers for the CLEAN-SC ($He < 2$) and OB ($He < 3$) algorithms. The weak performance of Orthogonal Beamforming at low frequencies is in line with the observations discussed by Sarradj [5].

In the evaluated Helmholtz number range, the DAMAS and the CMF algorithms both perform similarly with the median never deviating more than 3 dB from zero for the specific level error of the strongest source. At low He, the DAMAS error has a higher absolute value than the CMF error. The latter, however, features a broader spread and for a significant portion of the cases, the level error is positive, i.e., the source levels are overestimated.

For secondary sources up to the weakest source in the data sets, the errors increase in terms of spread and deviation of the median from zero. The CMF error has a higher magnitude than the DAMAS error for the weakest sources.

All methods except OB appear to reach optimum performance around $He = 4$. At higher Helmholtz numbers, the level error median again drops below zero for DAMAS, CLEAN-SC and CMF, and a higher spread of values can be seen. Contrary to this, the Orthogonal Beamforming error spread diminishes with increasing Helmholtz number, and the level of the median stays constant, albeit at -1 dB.

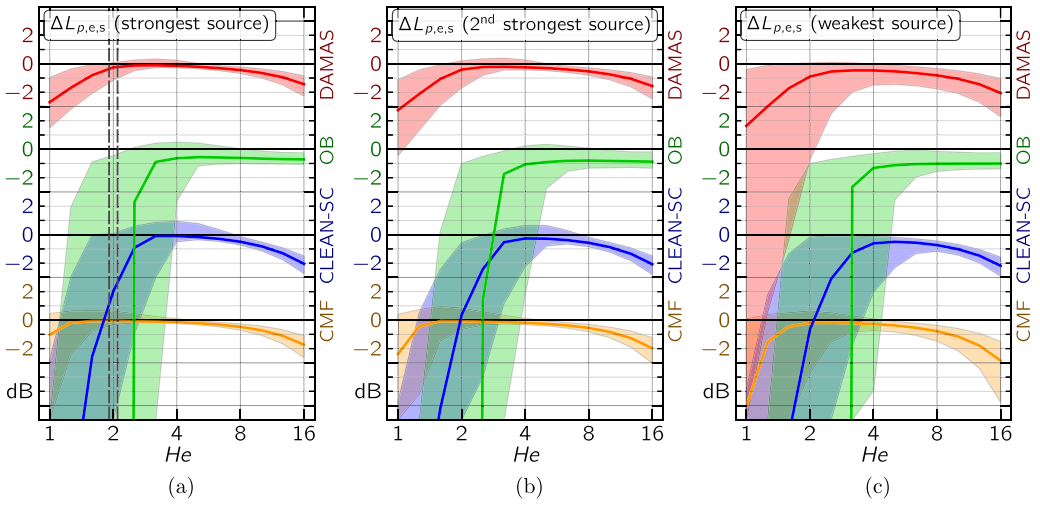

Fig. 9. Helmholtz number dependency of the specific level error $\Delta L_{p,e,s}$ for (a) the strongest, (b) the second-strongest, and (c) the weakest source in each data set. The colored lines show the median of all calculated level errors for the respective methods, and the filled areas represent the interval between the 16th and 84th percentiles. The dashed lines around $He = 2$ in sub-figure (a) mark the case evaluated in more detail in Fig. 8.

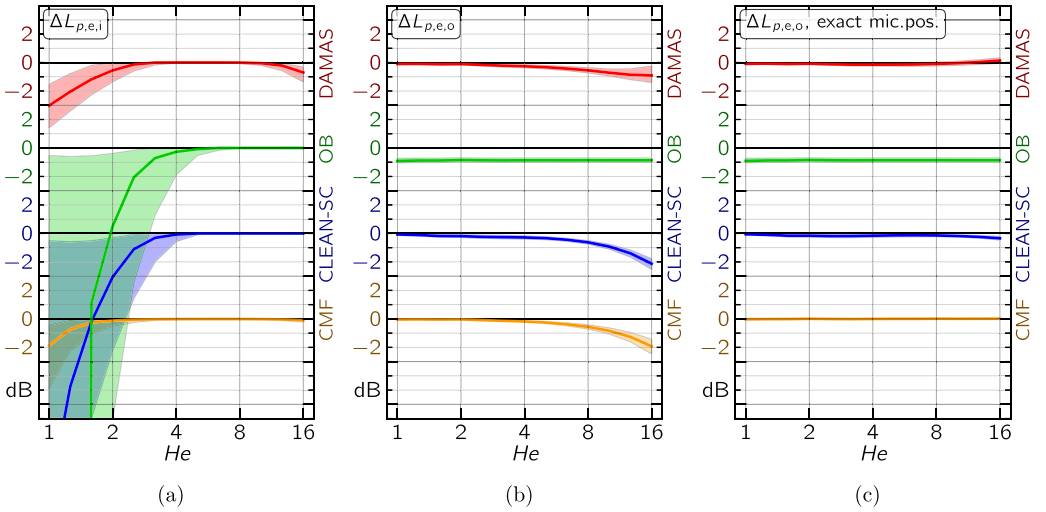

Fig. 10. Dependency on Helmholtz number: (a) inverse level error, (b) overall level error, (c) overall level error for data sets with non-distorted microphone positions.

From the specific level error plots in Fig. 9 it is not possible to deduce whether a negative value is caused by actually underestimating the source level or by the position of the source being calculated incorrectly. For this, examining the characteristics of the inverse and the overall level error and their dependency on the Helmholtz number can be of help.

As can be seen in Fig. 10a, the median and the dispersion of the inverse level error $\Delta L_{p,e,i}$ show approximately the same trends for all methods at low *He* as the specific level errors. This means that the combined levels inside the integration areas at the source positions are lower than the overall sound pressure level, i.e., there are sources being reconstructed at positions different from the actual present sources. At higher *He*, the inverse level error approaches zero, indicating that the reconstructed source levels are appearing at the correct positions. One exception to this is the DAMAS algorithm, where the error drops below zero again for $He > 10$.

The overall level error $\Delta L_{p,e,o}$ (Fig. 10b) is at zero (or, for OB, constantly at -1 dB) for $He \leq 4$. For higher Helmholtz numbers, the deviation from zero and the dispersion of error increase for DAMAS, CLEAN-SC and CMF. The reason for that becomes apparent when the same error is plotted for the data sets being generated without distortion of the microphone positions [17] (Fig. 10c): for "perfect" data, the overall level error stays at zero.

This illustrates the sensitivity of the algorithms to imperfections in the assumed sound path or misplacements of the microphones. Interestingly, the median of the deviation differs between the methods. At $He = 16$, the DAMAS error median is at about -1 dB, while for CLEAN-SC and CMF, the error is at about -2 dB. The Orthogonal Beamforming result appears not to be affected by the distorted microphone positions, at least at high Helmholtz numbers. This can be explained by the nature of the algorithm, which bases the positioning of the sources on delay-and-sum beamforming, but assigns eigenvalues from the eigen-decomposition of the CSM to the found positions, whereas the other algorithms rely on the evaluation of the phase differences between the microphones, which become more erroneous at higher Helmholtz numbers, when the model is not perfectly met.

In general, it can be reasonably assumed that reconstructed sources tend to be wrongly positioned at lower Helmholtz numbers ($He < 4$), while for $He > 4$ (with the exception of OB), the source level is more likely to be underestimated.

4.2.2. *Influence of number of sources*

For all methods, the dispersion of the specific level error increases with higher number of sources in one data set. As is shown in Fig. 11, the extent of the dispersion is similar between the methods for $He = 16$ and $He = 8$, but much higher for CLEAN-SC and OB for $He = 4$.

Interestingly, with more than 4 sources at $He = 4$ and more than 6 sources at $He = 8$, there is a considerable amount of cases where the specific level error is positive, i.e., the source level is overestimated.

However, it has to be kept in mind that for the specific level error, each source is rated separately and relative to its own expected level. Therefore, in one data set, there may be several positive $\Delta L_{p,e,s}$ level errors for secondary sources and one negative $\Delta L_{p,e,s}$ of lower magnitude for a louder source, and no or even a negative overall level error.

This can be seen in Fig. 12a. At $He = 8$, with a median between 0 and -1 dB, the overall level error exhibits almost no dependency on the number of sources, and has a very low dispersion of values. Only for DAMAS, the magnitude of error median increases slightly when more sources are present. This trend becomes more distinct for $He = 16$ (Fig. 12b), where the DAMAS $\Delta L_{p,e,o}$ median drops from $+1$ dB for one source to -2 dB for 10 sources. Except for a minor variation of the $\Delta L_{p,e,o}$ median for the CMF algorithm, the error stays constant for the other algorithms at this Helmholtz number.

The magnitude of inverse level error at $He = 16$ increases with decreasing number of sources in the case of DAMAS, whereas it

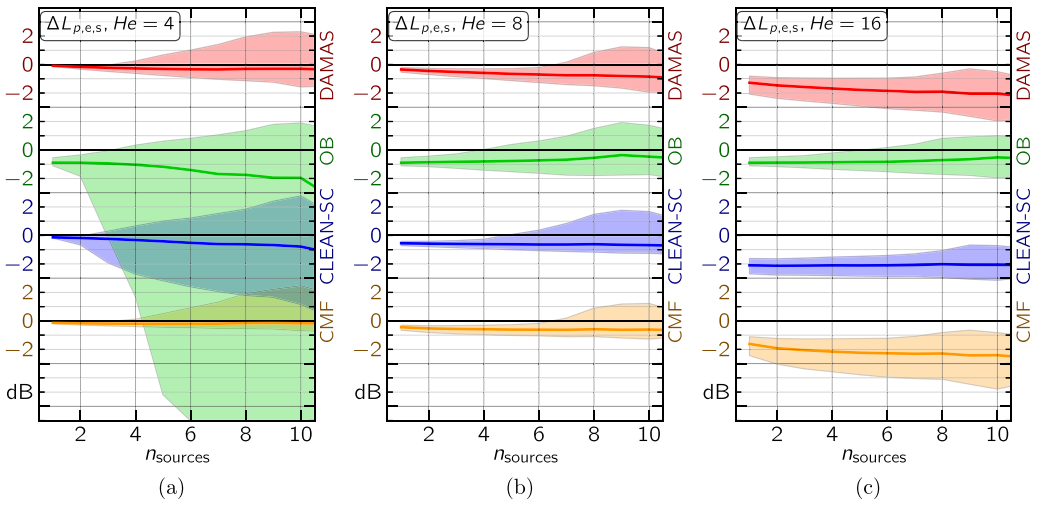

Fig. 11. Dependency on number of sources: specific level error for (a)*He* = 4, (b) *He* = 8, (c) *He* = 16.

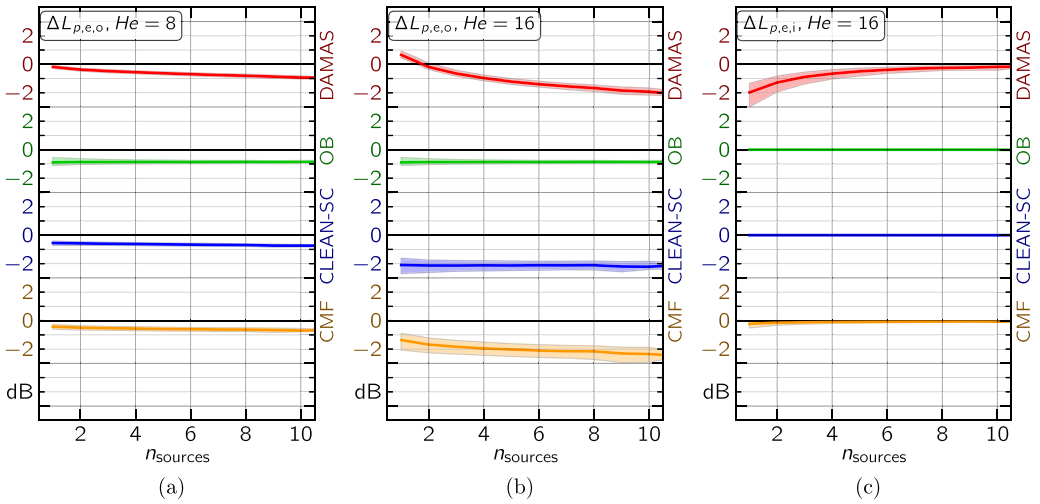

Fig. 12. Dependency on number of sources: overall level error for (a) *He* = 8, (b) *He* = 16; (c): inverse level error for *He* = 16.

stays at 0 dB for the other algorithms (Fig. 12c). This means that while with more sources, DAMAS tends to underestimate the overall source level, with less sources, this algorithm is more likely to reconstruct sources apart from actual source positions.

4.2.3. Influence of relative source levels

An important task for an array method is the correct reconstruction of multiple sources. As is shown in the following, the algorithm performance is also influenced by the relative properties of the sources in the data set, i.e., their relative level and positioning.

Fig. 13 shows the specific level error of a source depending on the level difference of that source to the strongest one in its data set. At *He* = 4 (Fig. 13a), OB shows the largest dispersion of values, while the median stays mostly constant slightly below $\Delta L_{p,e,s} = -1$ dB. The CLEAN-SC error has less dispersion, and the error median always stays between 0 and -1 dB in the evaluated interval of $0 > \Delta L_{p,\text{strongest}} >= -15$ dB, its magnitude slowly increasing with larger level differences. DAMAS and CMF show almost no error at small level deviations. However, with increasing level difference the error median drops further below zero and the dispersion increases for both algorithms. This means that these algorithms will most likely underestimate the level of sources that are secondary in a given setup. The magnitude of the specific level error is larger for DAMAS than for CMF at *He* = 4.

At *He* = 16 (Fig. 13b), the minimum error corresponds to the level errors visible in Fig. 9 at this Helmholtz number. Orthogonal Beamforming performs better than at *He* = 4, with the median at $\Delta L_{p,e,s} = -1$ dB and a low dispersion of values. While the rate at which the magnitude of the level error median increases is similar to the case at *He* = 4 for DAMAS and

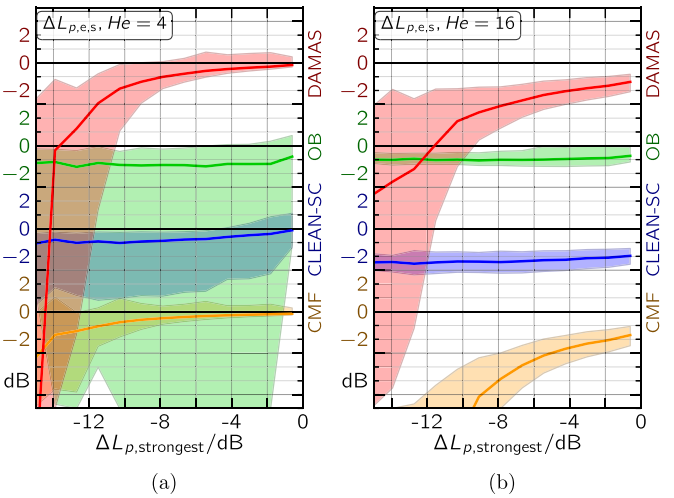

Fig. 13. Specific level error depending on the level difference to the strongest source in the data set for (a) $He = 4$ and (b) $He = 16$.

CLEAN-SC, the CMF level error drops much faster here. Thus, not only will CMF underestimate the level of minor sources, but also the reconstructed spectrum of this source will be distorted, favoring lower frequencies.

4.2.4. *Influence of source positions*

The influence of the positioning of the sources on the reconstruction ability of the algorithms is illustrated in Figs. 14 to 16.

Fig. 14 shows $\Delta L_{p,e,s}$ for the sources depending on the distance to the closest other source in the respective data set. At $He = 2$ and $He = 4$ (Fig. 14a and b), all methods perform better with the sources being farther apart, with a level error median between 0 and -0.5 dB, and a very low dispersion of values. At smaller source distances, the magnitude of the specific level error and its dispersion increases for all methods. For CLEAN-SC and OB, this happens more drastically and already at higher $\Delta r_{\min}$ as for DAMAS and CMF, which do not show a significant level error at $He = 4$. The trend of the negative error median is reversed for source distances below 0.1 d, where it increases and even becomes positive. This is explained by the integration circles around the two sources overlapping, so that the integration area of one source includes focus points that are attributed to the other source as well.

At $He = 16$ (Fig. 14c), the specific level error has a higher magnitude for DAMAS, CLEAN-SC and CMF over the whole range of $\Delta r_{\min}$. In contrast to lower Helmholtz numbers, here, the median diverges more and more from 0 dB with higher source distances, reaching values around $\Delta L_{p,e,s} = -3$ dB at $\Delta r_{\min} = 0.8$ d. The exception is the OB algorithm, where the error median does not fall below -1 dB and its magnitude decreases with larger distances.

For a good reconstruction, it is therefore generally of advantage to have the source as far from the other sources as possible at low to medium Helmholtz numbers. At higher He, however, sources being farther apart lead to higher error magnitudes for DAMAS, CLEAN-SC and CMF.

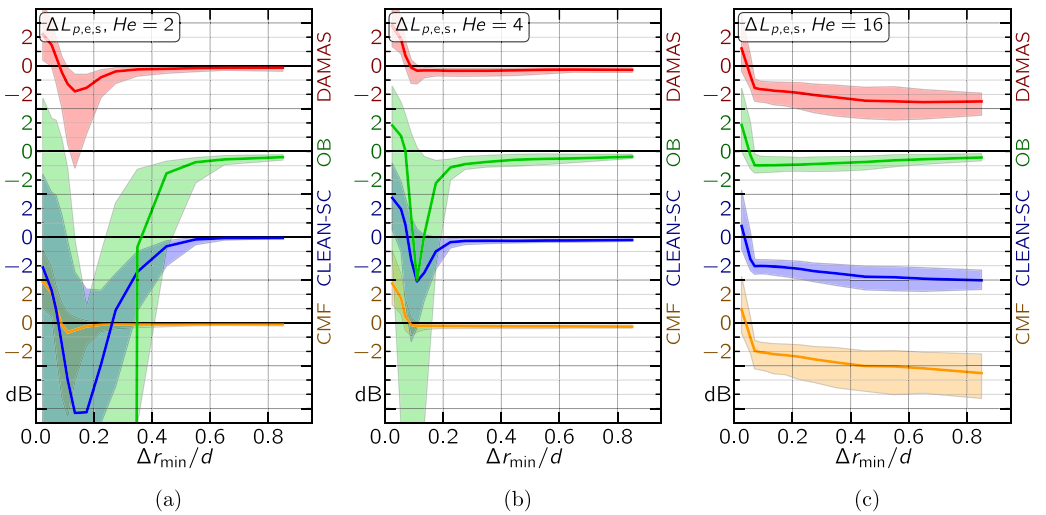

Fig. 14. Specific level error depending on the distance to the closest source: (a) $He = 2$, (b) $He = 4$, (c) $He = 16$.

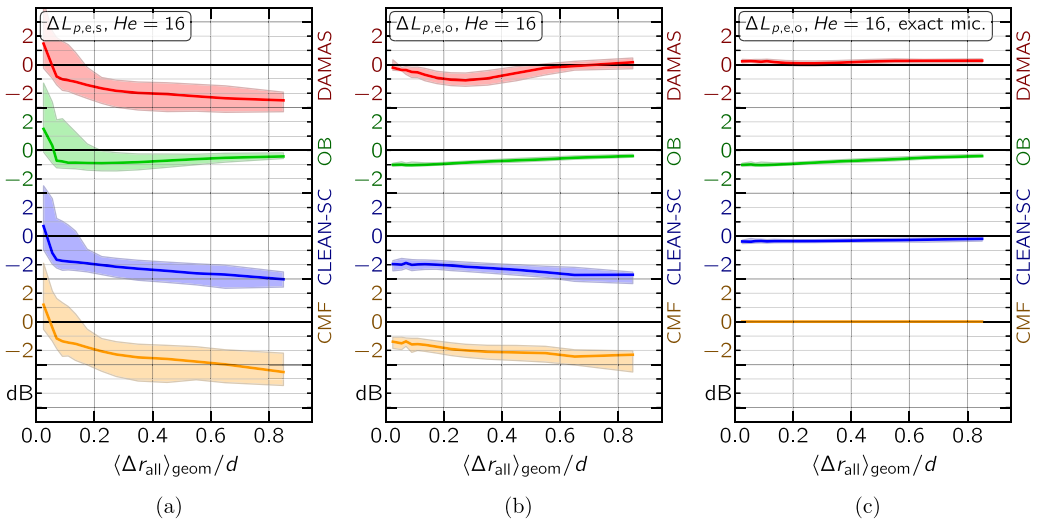

Fig. 15. Dependency on "source scattering" (geometric mean of all source distances in one data set) at $He = 16$: (a) specific level error, (b) overall level error, (c) overall level error with undistorted microphone positions.

The same trend can be observed regarding the specific level error depending on the geometric mean of the distances of all sources in one data set $\langle \Delta r_{\mathrm{all}} \rangle_{\mathrm{geom}}$, as is done for $He = 16$ in Fig. 15a. The geometric mean of the distances can be used as a measure for the general scatter of the source positions in one data set, i.e., the higher $\langle \Delta r_{\mathrm{all}} \rangle_{\mathrm{geom}}$, the more the sources are scattered over the focus area. This is somewhat similar to the minimum distance of the sources, but allows the evaluation per-data-set when more than two sources are present, which is necessary for the overall and inverse level error.

As is visible in Fig. 15b, the overall level error follows a similar trend as the specific level error for OB, CLEAN-SC and CMF. The strong increase at distances below 0.5 d is not visible here, since the sources are not regarded separately and there is no overlapping integration areas. The increasing magnitude of the level error for CLEAN-SC and CMF shows that with a higher source scattering, the overall level is underestimated to a greater extent. As is shown in Fig. 15c, this does not occur when using data simulated with a flawless transfer path.

While the DAMAS specific level error shows the same trend as CLEAN-SC and CMF, the median of the overall level error approaches 0 dB for high $\langle \Delta r_{\mathrm{all}} \rangle_{\mathrm{geom}}$ after an initial decrease. In case of the DAMAS algorithm, therefore, the imperfect positioning of the microphones does not lead to systematically underestimating the overall source levels with higher source scattering, but to either a false localization or the reconstruction of spurious sources. The decreasing inverse level error as shown in Fig. 16c confirms this.

Aside from the inverse level error caused by the mis-allocation of source levels with the DAMAS algorithm at higher Helmholtz numbers and higher source scattering, the magnitude of inverse level error also increases for lower He and $\langle \Delta r_{\mathrm{all}} \rangle_{\mathrm{geom}}$ (Fig. 16a and b). This corresponds to what can be seen in Figs. 14a and b. Since $\Delta L_{p,\mathrm{e,i}}$ approaches 0 dB again when

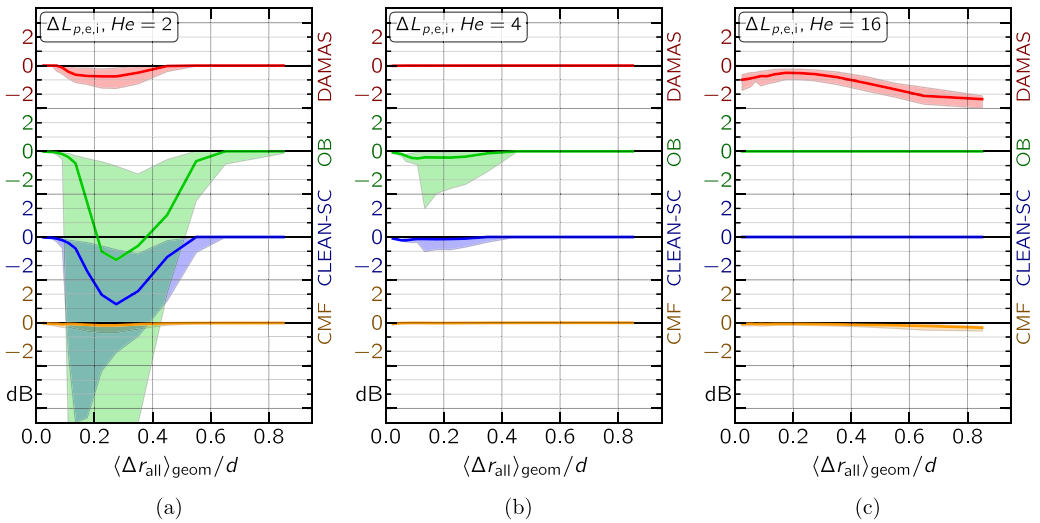

Fig. 16. Dependency of the inverse level error on the source scattering: (a) $He = 2$, (b) $He = 4$, (c) $He = 16$.

the scattering becomes so small that the integration circles overlap, it can be concluded that the localization error is solely caused by the reduced resolution capability of the algorithms at lower Helmholtz numbers and that neighboring sources are reconstructed as one source. The error is especially large for CLEAN-SC and OB, which, at $He = 2$, exhibit an inverse level error median up to -4.5 dB and -7.5 dB respectively.

5. Conclusion

A method for assessing the reliability of microphone array methods has been presented. The idea is to provide a framework that allows rating the method performance depending on various parameters. Since the possible parameter space is extensive and the objective is to cover a broad range of possible applications, a statistical approach was chosen to generate data sets onto which the methods are applied.

For quantifying the reliability of a method, error measures were defined which derive the deviation of the expected from the actual result from the calculated sound source maps. These errors were then evaluated statistically and plotted against varying parameters, allowing the assignment of a characteristic error to a given parameter range. The basic methodology can be summarized as follows:

1. Define boundary conditions for the intended use case.
2. Make assumptions on the nature of possible parameter variations.
3. Perform Monte Carlo simulations.
4. Process simulated data sets with microphone array methods.
5. Apply rating criteria on the results and study performance.

The parameter dependencies studied in this paper include the dimensionless frequency (Helmholtz number), the number of sources, the source positions, the source levels, and derived quantities, such as source distances or level differences.

In this study, four different methods with fixed method-specific parameters were compared: DAMAS, OB, CLEAN-SC, and CMF. While often exhibiting comparable overall trends, differences in the performance of algorithms may be considerable in terms of error magnitude for certain parameter combinations. All methods generally perform comparably well at Helmholtz numbers around 4. At lower *He*, DAMAS and CMF outperform the other algorithms, while at higher *He*, OB proves to be the most stable method, it being the algorithm the least sensitive to deviations from the assumed sound propagation but also delivering unreliable results at lower Helmholtz numbers.

DAMAS and CMF show better reconstruction results for sources close to each other than the other two methods. However, they tend to systematically underestimate the reconstructed level for secondary sources, which is not the case with CLEAN-SC and OB. In general, all algorithms benefit of sources being farther apart. However, this is no longer true for higher *He*, where only OB is capable of reconstructing the correct source level and position.

Applied on a given setup with known boundary conditions, this study provides a tool to evaluate the reliability of the results calculated with a certain method. While the objective was to generate a case as universal as possible, the used setup is still exemplary in many respects. Nevertheless, the underlying data generation and evaluation framework is applicable for arbitrary setups with differing array geometries, source areas, source types etc.

A drawback of this evaluation principle is that, because of the necessary generation of data sets and the subsequent application of the array methods, it requires considerable computation time prior to the actual evaluation. This motivates the careful definition of the boundary conditions governing the data generation with regard to intended actual experiments. On the other hand, the framework allows the flexible adaptation of any component in the data generation for taking into account other parameters of interest.

Possible enhancements for future studies include the evaluation of method performance with sources spread over a larger area (i.e., not only point sources) and partial or full correlation of sources to cover more realistic scenarios.

Acknowledgment

The authors thankfully acknowledge the support of this research by *Deutsche Forschungsgemeinschaft* through grant SA 1502/5-1.

References

[1] T. J. Mueller, (Ed), Aeroacoustic Measurements, Springer, Berlin, Heidelberg, 2002, http://dx.doi.org/10.1007/978-3-662-05058-3.
[2] R.P. Dougherty, Functional beamforming, in: Proceedings of the 5th Berlin Beamforming Conference, Berlin, 2014, pp. 1–25.
[3] T.F. Brooks, W.M. Humphreys, A deconvolution approach for the mapping of acoustic sources (DAMAS) determined from phased microphone arrays, J. Sound Vib. 294 (4–5) (2006) 856–879, http://dx.doi.org/10.1016/j.jsv.2005.12.046.
[4] P. Sijtsma, CLEAN based on spatial source coherence, Int. J. Aeroacoustics 6 (4) (2007) 357–374, http://dx.doi.org/10.1260/147547207783359459.

[5] E. Sarradj, A fast signal subspace approach for the determination of absolute levels from phased microphone array measurements, J. Sound Vib. 329 (9) (2010) 1553–1569, http://dx.doi.org/10.1016/j.jsv.2009.11.009.
[6] D. Blacodon, G. Elias, Level estimation of extended acoustic sources using a parametric method, J. Aircr. 41 (6) (2004) 1360–1369, http://dx.doi.org/10.2514/1.3053.
[7] T. Yardibi, J. Li, P. Stoica, L.N. Cattafesta, Sparsity constrained deconvolution approaches for acoustic source mapping, J. Acoust. Soc. Am. 123 (5) (2008) 2631–2642, http://dx.doi.org/10.1121/1.2896754.
[8] G. Herold, E. Sarradj, Preliminary benchmarking of microphone array methods, in: Proceedings of the 5th Berlin Beamforming Conference, Berlin, 2014, pp. 1–13.
[9] T. Yardibi, N.S. Zawodny, C. Bahr, F. Liu, Comparison of microphone array processing techniques for aeroacoustic measurements, Int. J. Aeroacoustics 9 (6) (2010) 733–762, http://dx.doi.org/10.1260/1475-472X.9.6.733.
[10] Z. Chu, Y. Yang, Comparison of deconvolution methods for the visualization of acoustic sources based on cross-spectral imaging function beamforming, Mech. Syst. Signal Process. 48 (1–2) (2014) 404–422, http://dx.doi.org/10.1016/j.ymssp.2014.03.012.
[11] Q. Leclere, A. Pereira, C. Bailly, J. Antoni, C. Picard, A Unified formalism for acoustic imaging techniques: illustrations in the frame of a didactic numerical benchmark, in: Proceedings of the 6th Berlin Beamforming Conference, Berlin, 2016, pp. 1–17.
[12] K. Ehrenfried, L. Koop, Comparison of iterative deconvolution algorithms for the mapping of acoustic sources, AIAA J. 45 (7) (2007) 1584–1595, http://dx.doi.org/10.2514/1.26320.
[13] H.L. Van Trees, Detection, Estimation, and Modulation Theory, Part IV, Optimum Array Processing, John Wiley & Sons, Inc., New York, USA (2002) http://dx.doi.org/10.1002/0471221104.
[14] R. Dougherty, R. Ramachandran, G. Raman, Deconvolution of sources in aeroacoustic images from phased microphone arrays using linear programming, Int. J. Aeroacoustics 12 (7–8) (2013) 699–718, http://dx.doi.org/10.1260/1475-472X.12.7-8.699.
[15] C.M. Sparrow, On spectroscopic resolving power, Astrophys. J. 44 (76) (1916) 76, http://dx.doi.org/10.1086/142271.
[16] G. Herold, E. Sarradj, T. Geyer, Covariance Matrix Fitting for Aeroacoustic Application, in: AIA-DAGA 2013 Conference on Acoustics, Merano, March 2013, pp. 1926–1928.
[17] G. Herold, E. Sarradj, An approach to estimate the reliability of microphone array methods, in: Proceedings of the 21st AIAA/CEAS Aeroacoustics Conference, Dallas, June 2015, pp. 1–10. http://dx.doi.org/10.2514/6.2015-2977.
[18] D.H. Johnson, D.E. Dudgeon, Array Signal Processing: concepts and Techniques, Prentice Hall, Englewood Cliffs, 1993.
[19] P.D. Welch, The use of fast fourier transform for the estimation of power spectra: a method based on time averaging over short, modified periodograms, IEEE Trans. Audio Electroacoustics 15 (2) (1967) 70–73, http://dx.doi.org/10.1109/TAU.1967.1161901.
[20] E. Sarradj, Three-dimensional acoustic source mapping with different beamforming steering vector formulations, Adv. Acoust. Vib. 2012 (2012) 1–12, http://dx.doi.org/10.1155/2012/292695.
[21] R. Tibshirani, I. Johnstone, T. Hastie, B. Efron, Least angle regression, Ann. Stat. 32 (2) (2004) 407–499, http://dx.doi.org/10.1214/009053604000000067.
[22] H. Zou, T. Hastie, R. Tibshirani, On the degrees of freedom of the lasso, Ann. Stat. 35 (5) (2007) 2173–2192, http://dx.doi.org/10.1214/009053607000000127.
[23] Acoular - Acoustic testing and source mapping software, ⟨http://www.acoular.org⟩, (accessed 11.01.2017).
[24] E. Sarradj, G. Herold, A Python framework for microphone array data processing, Appl. Acoust. 116 (2017) 50–58, http://dx.doi.org/10.1016/j.apacoust.2016.09.015.